

Thermal conductivity and tunable thermal anisotropy of magnetic CrSBr monolayer

Marta Loletti,[†] Alejandro Molina-Sánchez,[‡] Juan Sebastián Reparaz,[†] Xavier Cartoixà,[¶] and Riccardo Rurali^{*,†}

[†]*Institut de Ciència de Materials de Barcelona, ICMA-B-CSIC, Campus UAB, 08193 Bellaterra, Spain*

[‡]*Institute of Materials Science (ICMUV), University of Valencia, Catedrático Beltrán 2, E-46980 Valencia, Spain*

[¶]*Departament d'Enginyeria Electrònica, Universitat Autònoma de Barcelona, Bellaterra, 08193, Barcelona, Spain*

E-mail: rrurali@icmab.es

Abstract

We present first-principles calculations of the thermal conductivity, κ , of monolayer CrSBr, a van der Waals magnetic 2D material. We find a considerable thermal anisotropy, with a ratio κ_{xx}/κ_{yy} of around 1.8. The anisotropy stems from a combined effect of phonon velocities and lifetimes and can be tuned by controlling the flake size by suppressing long mean path phonons.

Introduction

The advent of two-dimensional materials (2DMs)¹⁻³ has opened up many exciting possibilities, including channels for field effect transistors with improved gate control,⁴ van der Waals

heterostructures⁵ for efficient photodetectors,² and non-volatile spintronic memories.⁶ With the progressive prediction and synthesis of 2DMs featuring different possible electronic properties (i.e., metallic, semiconductor, topological insulators) as long-established 3D material counterparts, it was only a matter of time until the first single-/few-layer magnetic 2DMs⁷ were experimentally found, namely CrGeTe₃⁸ and CrI₃.⁹ Since then, many others have been added to the catalog of 2D magnets¹⁰ and they are now the focus of an intense research activity. A question that naturally arises is how the magnetic order couples to other physical properties. Telford *et al.*¹¹ have found that the magnetoresistance presents clear signatures of the underlying magnetic order, whereas Peng *et al.*¹² showed that the spin orientation and the metamagnetic transitions in CrPS₄ can be controlled by hydrostatic pressure. The interplay of magnetism and thermal transport properties in 2D magnets, however, is an area that has received little attention so far.

Among van der Waals magnetic materials, CrSBr stands out due to robust magnetism, air-stability, strong anisotropy, and quasi one-dimensional electron transport.¹³ Similar to other 2D magnetic materials (e.g. CrI₃), in CrSBr each layer is ordered ferromagnetically and couples antiferromagnetically with the other layers.¹⁴ Due to the interest sparked by these properties, very recently CrSBr thermal transport properties have been the focus of a few theoretical studies, but the results feature a huge variability. Xuan *et al.*¹⁵ reported an ultralow lattice thermal conductivity, κ , for CrSX (X = Cl, Br, I) monolayers (MLs), as obtained from density-functional theory calculations (DFT) and the solution of the Boltzmann Transport Equation (BTE). Although they reported values of κ *above* the Curie temperature of ML CrSBr (experimentally estimated to be 146 K by Lee *et al.*¹⁴), by roughly extrapolating their results at 200 K down to lower temperatures, one obtains $\kappa_{xx} \approx 0.8 \text{ W m}^{-1}\text{K}^{-1}$ and $\kappa_{yy} \approx 0.3 \text{ W m}^{-1}\text{K}^{-1}$. More recently, however, Liu *et al.*¹⁶ reported significantly larger values, 25.48 and 11.90 $\text{W m}^{-1}\text{K}^{-1}$ at 150 K for κ_{xx} and κ_{yy} , respectively. This difference is striking, because both groups use the same DFT code and exchange-correlation functional. The linearized BTE, on the other hand, is solved with ShengBTE¹⁷ in one case and

phono3py¹⁸ in the other, but a recent comparative study allows ruling out that this different choice could originate sizeable discrepancies.¹⁹ Larger thermal conductivities –yet of the same order of magnitude as those of Ref. 16– have been obtained by Han and coworkers,²⁰ who report values of 80.79 and 37.38 W m⁻¹K⁻¹ at 145 K. In this work, a machine learning force-field is trained on DFT datasets and then used to compute harmonic and anharmonic force constants. Noteworthy, this study included both three- and four-phonon scattering, thus accounting for one additional scattering mechanism. Yet, they found larger κ than Liu and coworkers,¹⁶ who only considered anharmonicity up to the third-order.

Here we revisit the calculation of the thermal conductivity of ML CrSBr, focusing our attention on the anisotropy of heat transport. We first study the robustness of the ferromagnetic (FM) ground-state and explore the possibility of observing a strain-induced phase transition, where the antiferromagnetic (AFM) ordering can become favored, considering both uniaxial and biaxial strain conditions. This would be an important feature, because one could in principle selectively access both magnetic phases by triggering an AFM \rightarrow FM transition with an external magnetic field. We then present a detailed analysis of the thermal conductivity of ML CrSBr, studying both the dependence on temperature and on the flake size and shedding light on the reason of the anisotropy of the in-plane thermal conductivity. Finally, we highlight how dimensional confinement can be used as a control knob to tune the anisotropy of heat transport.

Computational Methods

Calculations have been carried out within density functional theory (DFT)^{21,22} as implemented in the Vienna *ab initio* simulation package,²³ with the projector augmented wave (PAW) pseudopotential method and a plane-wave cutoff of 520 eV. The exchange-correlation energy was described by the Perdew-Burke-Ernzerhof (PBE)²⁴ functional within the framework of the generalized gradient approximation (GGA), and the long-range dispersion in-

teractions were included through van der Waals corrections described in the framework of Grimme’s approach with zero-damping function (DFT-D3).²⁵ To properly describe the localized d -electrons of the transition-metal atoms, we employed the DFT+U approach as implemented in the VASP code. The on-site Coulomb interaction was treated using the simplified rotationally invariant formalism of Dudarev *et al.*²⁶ and the correction was applied with an effective Hubbard parameter $U_{eff} = 4.0$ eV.^{16,27} The monolayer was modeled using approximately 20 Å vacuum along the out-of-plane, \mathbf{c} -direction to avoid spurious interactions between periodic images. A $12 \times 10 \times 1$ Monkhorst-Pack \mathbf{k} -grid was used for Brillouin zone integration. Convergence was reached when forces were lower than 0.005 eV/Å and stress lower than 0.03 kbar. Second- and third-order interatomic force constants— IFC2s and IFC3s, respectively—were used as input for the almaBTE suite²⁸ to iteratively solve the Boltzmann Transport Equation (BTE) beyond the relaxation time approximation (RTA). IFC2s and the subsequent phonon dispersion curves were computed by finite differences with the `phonopy` software,^{18,29} using a $6 \times 5 \times 1$ supercell. IFC3s were also computed by finite differences using the same supercell, with the `thirdorder.py` package.¹⁷ IFC2s were postprocessed with the `hiPhive` package³⁰ to enforce the constraints imposed by rotational sum rules, necessary to obtain the correct quadratic dispersion for the ZA modes in 2DMs.³¹ To reproduce the suppression of LO-TO splitting at the Γ -point in 2D materials,^{32–34} phonons dispersions are computed without including non-analytical corrections in their standard formalism.

To compute physically meaningful in-plane thermal conductivity, one must define an effective thickness of the ML, a choice that is subjected to certain degree of arbitrariness. In one-atom thick MLs, such as graphene and h-BN, the most widely adopted approach consists in taking as thickness the interlayer spacing in the bulk. ML CrSBr, on the other hand, is made of 4 atomic planes and another possible choice is taking the distance between the two outer Br planes, d (see Figure 1 and Table 1). However, this solution is impractical when it comes to compare the thermal conductivity of the ML with the one of few-layer

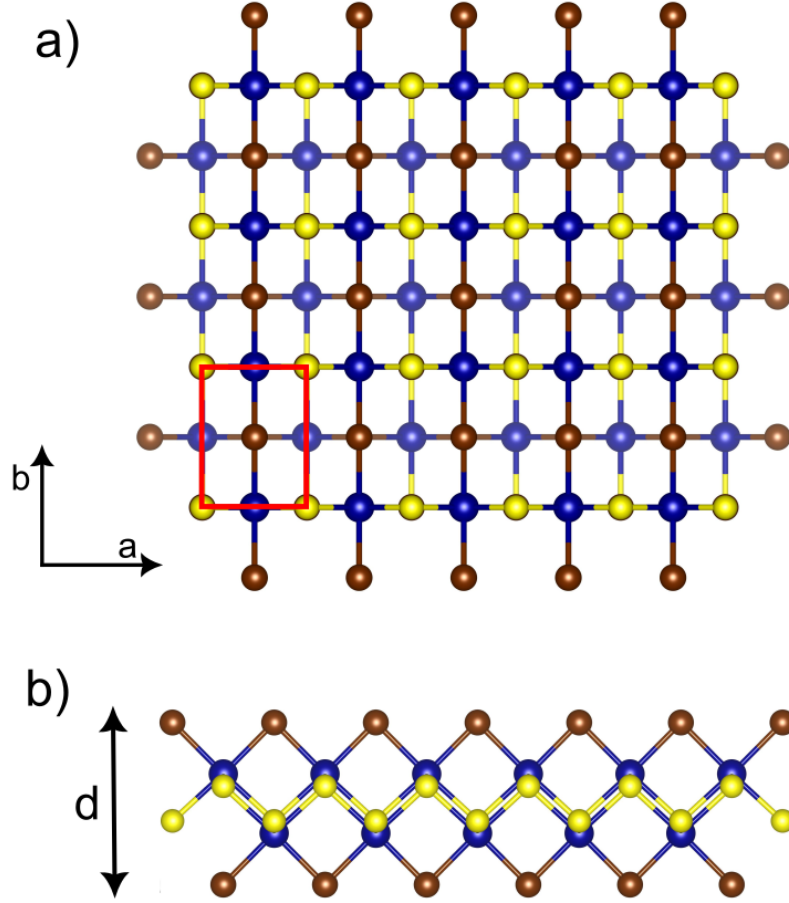


Figure 1: (a) Top and (b) side views of ML CrSBr; Cr, S, and Br atoms are represented by blue, yellow, and brown spheres, respectively; d indicates the distance between Br planes.

systems or bulk CrSBr. Therefore, we stick to the usual approach and take the interlayer separation as the effective ML thickness. To this end, we optimized the lattice vectors and atomic positions of bulk CrSBr with AA stacking and took the resulting \mathbf{c} -vector as the ML thickness.

Results

Ground-state and response to uniaxial and biaxial stress. At first we optimized the atomic positions and cell vectors of monolayer (ML) CrSBr in both the ferromagnetic

Table 1: Lattice parameters (a and b), ML thickness (d) and relative total energy for the FM and AFM configurations of ML CrSBr.

	AFM	FM
ΔE (meV/f.u.)	49	-
a (Å)	3.574	3.575
b (Å)	4.817	4.806
d (Å)	5.711	5.703

(FM) and antiferromagnetic (AFM) magnetic ordering, finding very similar lattice constants (see Table 1) and that the ground-state is FM ($\Delta E_{\text{FM-AFM}} = -49$ meV/f.u.), corroborating previous findings reported in the literature.^{14,35,36}

We then applied uniaxial tensile and compressive strain (ϵ) up to $\pm 5\%$ to the a and b lattice vectors, i.e. the x and y -axis, in order to investigate whether the application of an external uniaxial stress can lead to a modulation of the energy difference $\Delta E_{\text{FM-AFM}}$, and thus induce or ease a magnetic phase transition. In these calculations, the lattice vector perpendicular to the strained one is left free to relax and we found a positive Poisson's ratio, as in conventional non-auxetic materials (i.e., when one lattice vector is compressed, the other expands and viceversa). For each configuration, the total energies of the FM and AFM phases were computed, and the energy difference was monitored as a function of strain. In all cases, the FM state remains the most stable configuration, with $\Delta E_{\text{FM-AFM}}$ consistently negative across the entire strain range (see Supporting Information, Figure S1). This demonstrates that, within the investigated range, uniaxial mechanical deformation does not induce any magnetic phase transition in monolayer CrSBr, highlighting the robustness of its ferromagnetic ground state.

We further investigated the effect of strain by simultaneously applying it along both the a and b lattice directions to evaluate whether a combined deformation could alter the magnetic ground state of the CrSBr monolayer. Biaxial tensile and compressive strains were again applied in the range of $\pm 5\%$, and the total energies of the FM and AFM configurations were calculated for each strain level. Similar to the uniaxial case, the FM configuration remains

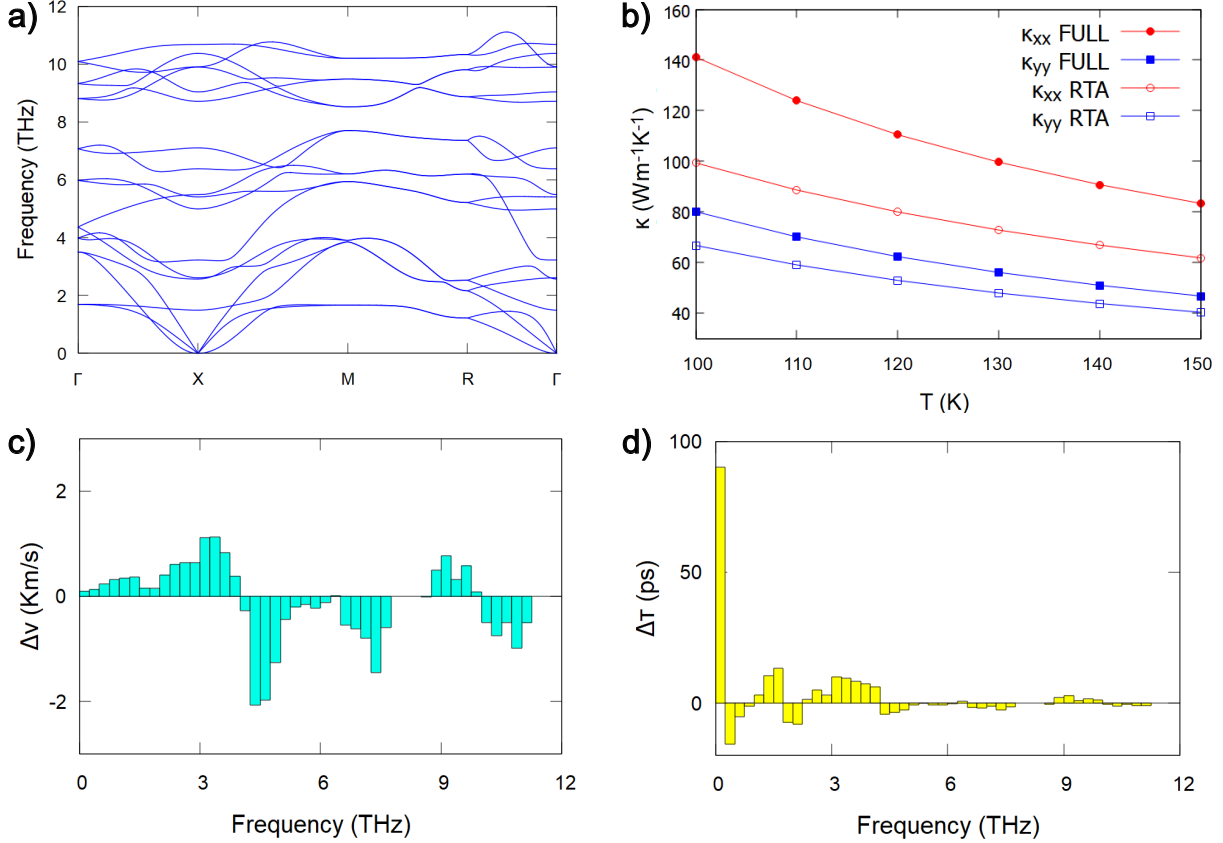


Figure 2: (a) Phonon dispersion. (b) Thermal conductivity as a function of temperature. (c) $\Delta v = v_x - v_y$ and (d) $\Delta\tau = \tau_x - \tau_y$ as a function of frequency; before subtraction, velocities and lifetimes were averaged over intervals of 1 THz. Phonon lifetimes, τ_i with $i = x, y$ (see text for definition) are computed at 150 K.

energetically favored over the AFM one throughout the entire strain range (Supporting Information, Figure S1). The energy difference $\Delta E_{\text{FM-AFM}}$ remains negative, confirming that no magnetic phase transition occurs under biaxial strain either. These results indicate that the ferromagnetic ground state of monolayer CrSBr is remarkably robust, being insensitive to both uniaxial and biaxial mechanical deformation within the studied strain range.

Phonon dispersion and anisotropic thermal conductivity. Once the ferromagnetic ground state of the ML was established, we investigated its in-plane thermal conductivity. The phonon dispersion is displayed in Figure 2a. At variance with previous results, where phonon bands next to the Γ point exhibit a small pocket of negative frequencies,^{15,16} by enforcing the rotational sum rules, we obtain the correct quadratic dispersion for the ZA

modes, as expected in 2DMs.³¹

The thermal conductivity, κ , was computed in the temperature range 100-150 K, where CrSBr is FM (the Curie temperature, above which CrSBr becomes paramagnetic, has been estimated to be 146-150 K^{14,37,38}). At such low temperatures heat transport is dominated by long wavelength phonons and convergence of the lattice thermal conductivity usually requires extremely dense \mathbf{q} -meshes to sample the Brillouin zone. We conducted a systematic convergence study (see Supporting Information, Figure S2) of κ_{xx} and κ_{yy} for samples of different characteristic sizes, L (namely, infinite, 10 μm , and 100 nm) and reached a robust convergence for a 100×100 \mathbf{q} -point grid. Our results for κ as a function of temperature are reported in Figure 2b. Therein, we also compare the predictions of the full solution of the phonon BTE^{28,39} with those obtained within the simplified RTA approach, finding that the latter provides completely unreliable values: not only the absolute values of κ_{xx} and κ_{yy} , but even the ratio between the two differ significantly from the results of the full solution (the error introduced by the RTA is particularly significant for κ_{xx} , i.e., $\approx 25\%$, almost twice as much the one for κ_{yy}). Indeed, as previously reported, in 2DMs⁴⁰⁻⁴² there is a significant fraction of phonon scattering events, involving phonon-phonon interaction, that do not restore first-order deviations from the equilibrium phonon distributions. Normal scattering events fall into this category, but some of the resistive processes do not restore to equilibrium small deviations of the phonon population along the transport direction⁴³ either. This has two consequences; (a) the RTA underestimates the thermal conductivity by treating some processes as resistive when they are not, as appreciable in Figure 2b, and (b) since individual phonons no longer diagonalize the scattering matrix, one cannot strictly speak of individual phonon contributions, or cumulative curves. Rather, one must resort to a partially collective description of the system,⁴⁴ or adopt a relaxon picture based on the diagonalization of the full scattering operator.⁴⁵ The fact that our calculations highlight a larger correction to the RTA on κ_{xx} is indicative that Normal processes in ML CrSBr would be dominated by phonons that predominantly travel along the x -axis.

Table 2: Thermal conductivities at 150 K, in $\text{W m}^{-1}\text{K}^{-1}$, for the different size configurations. Results are given for the RTA and the full solution of the BTE.

	RTA	BTE _{full}		RTA	BTE _{full}
$L = \infty$					
κ_{xx}^{FM}	61.83	83.38	$\kappa_{xx}^{\text{FM}}/\kappa_{yy}^{\text{FM}}$	1.53	1.78
κ_{yy}^{FM}	40.35	46.77			
$L = 10\mu\text{m}$					
κ_{xx}^{FM}	58.22	76.57	$\kappa_{xx}^{\text{FM}}/\kappa_{yy}^{\text{FM}}$	1.62	1.87
κ_{yy}^{FM}	35.85	40.99			
$L = 100\text{nm}$					
κ_{xx}^{FM}	21.01	23.09	$\kappa_{xx}^{\text{FM}}/\kappa_{yy}^{\text{FM}}$	1.67	1.77
κ_{yy}^{FM}	12.60	13.02			

Our results agree very well with those of Ref. 20. We found $\kappa_{xx} = 86.31 \text{ W m}^{-1}\text{K}^{-1}$ and $\kappa_{yy} = 43.08 \text{ W m}^{-1}\text{K}^{-1}$ at 150 K, somewhat larger than those of Han and coworkers (80.79 and $37.38 \text{ W m}^{-1}\text{K}^{-1}$ at 145 K), consistent with the fact that they took into account also higher-order anharmonic scattering processes.²⁰ The overall good agreement with their results, however, suggests that four-phonon processes in ML CrSBr are not a significant source of additional scattering.

The thermal conductivity is strongly anisotropic, with an anisotropy ratio κ_{xx}/κ_{yy} at 150 K of 1.8 (1.5 at the RTA level). In order to see whether the observed anisotropy can be traced back to a difference in phonon velocities, we computed $\Delta v = v_x - v_y$, where v_i is the i -component of the group velocity $\mathbf{v} = \partial\omega/\partial\mathbf{q}$. Indeed, we find that at low frequency, $\omega \lesssim 4 \text{ THz}$, $\Delta v > 0$ and thus $v_x > v_y$, in agreement with the larger value of κ_{xx} as compared to κ_{yy} . To factor in the role of anharmonicity via phonon lifetimes, we define $\tau_i = \tau \frac{v_i}{|\mathbf{v}|}$, where $i = x, y$, so that τ_i is the lifetime of phonons that predominately propagates along the i -axis. Similarly to what we did for the velocities, we computed $\Delta\tau = \tau_x - \tau_y$ and found that at very low frequency $\tau_x \gg \tau_y$, which again contributes to determine the κ anisotropy.

Anisotropy tuning through size modulation. When studying the thermal conductivity of a 2D material, it is indeed important to consider the dimensions of the flake system, since these directly influence heat transport at the microscopic level. The reason is that the

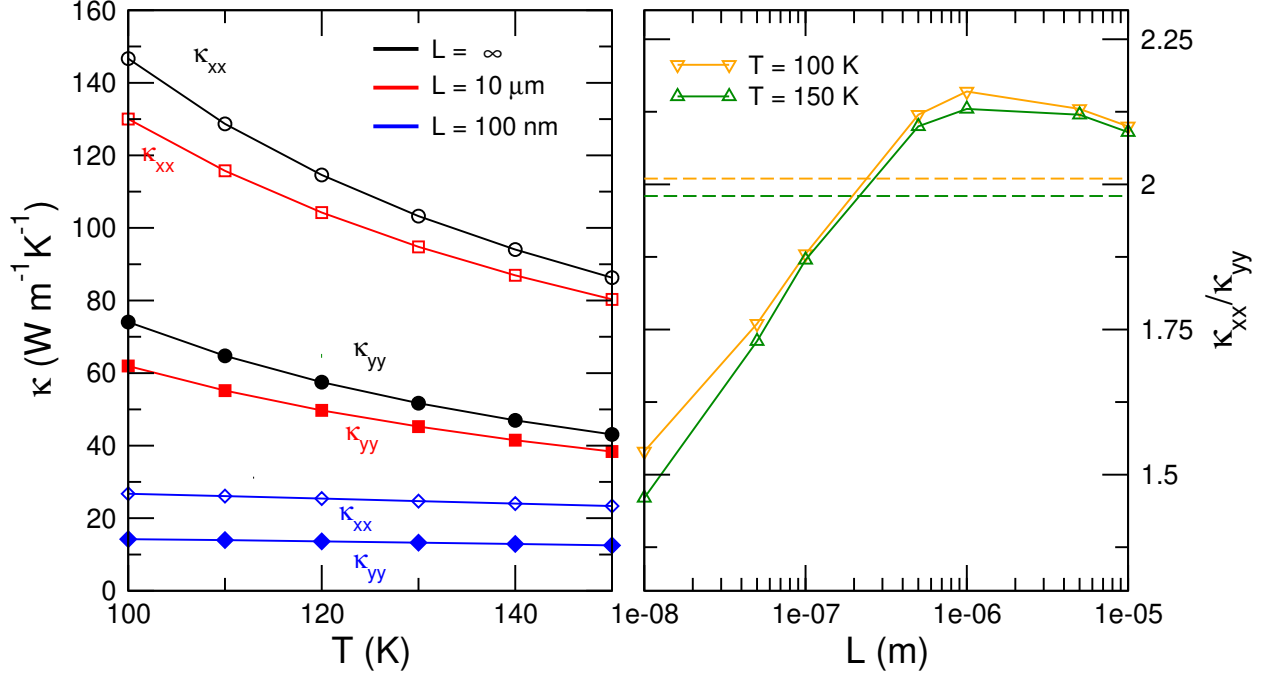


Figure 3: (Left) Thermal conductivity as a function of temperature of ML CrSBr of different characteristic size, L . (Right) Anisotropy ratio as a function of L at $T = 100$ and 150 K.

thermal conductivity is significantly influenced by the mean free path (MFP) of phonons. If the flake size is comparable to, or smaller than the MFP of a given set of phonons, the latter will be suppressed, giving rise to a boundary scattering term that must be accounted for. As a matter of fact, κ converges faster with the number of \mathbf{q} -points as sample size shrinks down (see Supporting Information, Figure S2), as very long-wavelength phonons progressively cease to contribute to κ when the sample dimensions are reduced.

Figure 3 displays κ_{xx} and κ_{yy} as a function of temperature of flakes of three selected sizes: $L = \infty$ (the infinite flake, same as in Figure 2b), $L = 10 \mu\text{m}$, and $L = 100 \text{ nm}$. The effect of boundary scattering in suppressing κ can be clearly appreciated, with values for the 100 nm flake 7 times smaller than for the unbounded sample. Additionally, we also found that Normal scattering processes are progressively suppressed when considering finite size effects and when $L = 100 \text{ nm}$ we almost recover the independent phonon picture consubstantial to the RTA (see Table 2).

The characteristic flake size, L , has also an effect on the anisotropy in thermal transport,

as shown in the right panel of Figure 3, where we plot the evolution of κ_{xx}/κ_{yy} as a function of the lateral dimension L of the sample. For small L values ($\sim 10^{-8}$ m), the ratio remains low, indicating a much less anisotropic thermal transport regime. As L increases, κ_{xx}/κ_{yy} progressively rises, staying around 2 and revealing that the intrinsic anisotropy of the material fully develops in the greater surface limit.

As discussed above, one of the reasons leading to $\kappa_{xx} > \kappa_{yy}$ in the infinite flake is that phonons propagating along the x -axis have longer lifetimes –and therefore larger MFPs– than those propagating along the y -axis. Consequently, when the flake size is uniformly reduced, one would expect boundary scattering to affect κ_{xx} sooner than κ_{yy} , since κ_{xx} is built up by phonons with longer MFPs. This is indeed what we observe if we repeat the analysis of Figure 2d in the case of smaller samples, e.g. $L = 10\mu\text{m}$ and $L = 100$ nm. The results shown in Figure 4, show that the large low-frequency peak in $\Delta\tau$ is progressively quenched as the sample size is reduced and that it vanishes at $L = 100$ nm. Notice though, that such a dependence with the sample size is not fully monotonic and that κ_{xx}/κ_{yy} exhibits a maximum around $L = 1\mu\text{m}$ (see Figure 3). This behavior stems from the role played by phonons with MFP between 0.2 and $1\mu\text{m}$ in determining the anisotropy, as shown in Figure 4d, where we plot the ratio between the cumulative thermal conductivity, κ_{xx} and κ_{yy} , as a function of the phonon MFP.

This behavior demonstrates that the thermal anisotropy can be effectively tuned by controlling the flakes dimensions. In the nanoscale regime, enhanced phononboundary scattering suppresses the in-plane thermal conductivity components differently along x and y , thereby reducing the overall anisotropy. Conversely, for larger flakes where boundary effects become negligible, the bulk anisotropy is restored. These results highlight that surface-area modulation offers a viable route to engineer the thermal anisotropy of layered materials, enabling control over heat transport properties via geometric confinement.

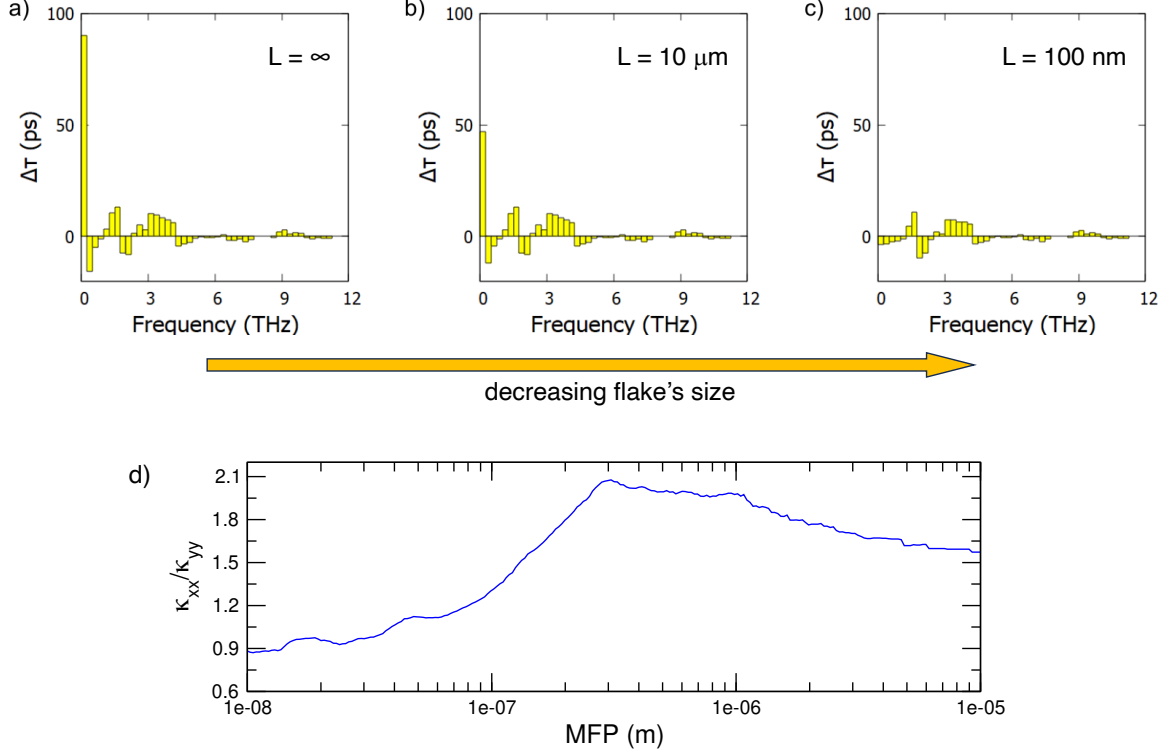


Figure 4: $\Delta\tau = \tau_x - \tau_y$ as a function of frequency for (a) $L = \infty$ (b) $10 \mu\text{m}$, and (c) 100nm ; before subtraction, lifetimes were averaged over intervals of 1 THz. Phonon lifetimes, τ_i with $i = x, y$ (see text for definition) are computed at 150 K. (d) Ratio between the cumulative thermal conductivity, κ_{xx} and κ_{yy} , as a function of the MFP, Λ , where $\kappa(\bar{\Lambda})$ is defined as the thermal conductivity considering only phonons with MFP $\Lambda < \bar{\Lambda}$.

Conclusions

In summary, we have computed the thermal conductivity of the ML CrSBr, finding κ_{xx} to be almost twice as large as κ_{yy} and tracing back this strong anisotropy to a combined effects of phonon velocities and phonon lifetimes. We also found that, by suppressing long MFP phonons, the anisotropy can be tuned to some extent by controlling the flake size. Our attempts to stabilize AFM ordering by means of tensile or compressive uni/biaxial strain were unsuccessful and ML CrSBr remains FM in all the conditions explored.

Acknowledgement

We acknowledge financial support by MCIN/AEI/10.13039/501100011033 under grant PDC2023-145934-I00, PID2024-162811NB-I00, PID2024-161603NB-I00, PID2023-146181OB-I00 and the Severo Ochoa Centres of Excellence Program under grant CEX2023-001263-S, and by the Generalitat de Catalunya under grant 2021 SGR 01519. This work is also supported by the Horizon Europe research and innovation program of the European Union under the Marie Skłodowska-Curie grant agreement 101118915 (TIMES). Calculations were performed at the Centro de Supercomputación de Galicia (CESGA).

Supporting Information Available

The data of unit cell relaxation, the interatomic force constants (IFCs) and other input/output files of the DFT and BTE calculations are freely available at dx.doi.org/10.5281/zenodo.18787296.

References

- (1) Novoselov, K. S.; Jiang, D.; Schedin, F.; Booth, T. J.; Khotkevich, V. V.; Morozov, S. V.; Geim, A. K. Two-dimensional atomic crystals. *Proceedings of the National Academy of Sciences* **2005**, *102*, 10451–10453.
- (2) Novoselov, K. S.; Mishchenko, A.; Carvalho, A.; Neto, A. H. C. 2D materials and van der Waals heterostructures. *Science* **2016**, *353*, aac9439.
- (3) Novoselov, K. S. Nobel Lecture: Graphene: Materials in the Flatland. *Rev. Mod. Phys.* **2011**, *83*, 837–849.
- (4) Radisavljevic, B.; Radenovic, A.; Brivio, J.; Giacometti, V.; Kis, A. Single-layer MoS₂ transistors. *Nature Nanotechnology* **2011**, *6*, 147–150.

- (5) Geim, A. K.; Grigorieva, I. V. Van der Waals heterostructures. *Nature* **2013**, *499*, 419–425.
- (6) Yang, H. et al. Two-dimensional materials prospects for non-volatile spintronic memories. *Nature* **2022**, *606*, 663–673.
- (7) Gibertini, M.; Koperski, M.; Morpurgo, A. F.; Novoselov, K. S. Magnetic 2D materials and heterostructures. *Nature Nanotechnology* **2019**, *14*, 408–419.
- (8) Gong, C.; Li, L.; Li, Z.; Ji, H.; Stern, A.; Xia, Y.; Cao, T.; Bao, W.; Wang, C.; Wang, Y.; Qiu, Z. Q.; Cava, R. J.; Louie, S. G.; Xia, J.; Zhang, X. Discovery of intrinsic ferromagnetism in two-dimensional van der Waals crystals. *Nature* **2017**, *546*, 265–269.
- (9) Huang, B.; Clark, G.; Navarro-Moratalla, E.; Klein, D. R.; Cheng, R.; Seyler, K. L.; Zhong, D.; Schmidgall, E.; McGuire, M. A.; Cobden, D. H.; Yao, W.; Xiao, D.; Jarillo-Herrero, P.; Xu, X. Layer-dependent ferromagnetism in a van der Waals crystal down to the monolayer limit. *Nature* **2017**, *546*, 270–273.
- (10) Wang, Q. H. et al. The Magnetic Genome of Two-Dimensional van der Waals Materials. *ACS Nano* **2022**, *16*, 6960–7079, PMID: 35442017.
- (11) Telford, E. J. et al. Coupling between magnetic order and charge transport in a two-dimensional magnetic semiconductor. *Nature Materials* **2022**, *21*, 754–760.
- (12) Peng, Y. et al. Controlling Spin Orientation and Metamagnetic Transitions in Anisotropic van der Waals Antiferromagnet CrPS4 by Hydrostatic Pressure. *Advanced Functional Materials* **2022**, *32*, 2106592.
- (13) Ziebel, M. E.; Feuer, M. L.; Cox, J.; Zhu, X.; Dean, C. R.; Roy, X. CrSBr: An Air-Stable, Two-Dimensional Magnetic Semiconductor. *Nano Lett.* **2024**, *24*, 4319–4329.

- (14) Lee, K.; Dismukes, A. H.; Telford, E. J.; Wiscons, R. A.; Wang, J.; Xu, X.; Nuckolls, C.; Dean, C. R.; Roy, X.; Zhu, X. Magnetic Order and Symmetry in the 2D Semiconductor CrSBr. *Nano Lett.* **2021**, *21*, 3511–3517.
- (15) Xuan, X.; Yang, Z.; Du, R.; Zhao, Y.; Yan, Y.; Liu, C.; Li, H.; Zhang, G. Ultralow thermal conductivity and anharmonic rattling in two-dimensional CrSX (X = Cl, Br, I) monolayers. *Mater. Adv.* **2023**, *4*, 4852–4859.
- (16) Liu, Y.; Zhi, Y.; Liu, Q.; Liu, Y.; Jiang, X.; Zhao, J. Lattice thermal conductivity in CrSBr: the effects of interlayer interaction, magnetic ordering and external strain. *J. Phys.: Condens. Matter* **2025**, *37*, 125701.
- (17) Li, W.; Carrete, J.; Katcho, N. A.; Mingo, N. ShengBTE: a solver of the Boltzmann transport equation for phonons. *Comp. Phys. Commun.* **2014**, *185*, 1747–1758.
- (18) Togo, A.; Chaput, L.; Tadano, T.; Tanaka, I. Implementation strategies in phonopy and phono3py. *J. Phys. Condens. Matter* **2023**, *35*, 353001.
- (19) McGaughey, A. J. H. et al. Phonon Olympics: Phonon property and lattice thermal conductivity benchmarking from open-source packages. *J. Appl. Phys.* **2025**, *138*, 135108.
- (20) Han, L.; Li, Z.; Tang, Z.; Wang, X.; Li, J.; He, C.; Tang, C.; Ouyang, T. Notable impact of magnetic order and flat phonon mode on the thermal transport properties of 2D magnetic semiconductor CrSBr. *J. Appl. Phys.* **2025**, *138*, 195101.
- (21) Hohenberg, P.; Kohn, W. Inhomogeneous Electron Gas. *Phys. Rev.* **1964**, *136*, B864–B871.
- (22) Kohn, W.; Sham, L. J. Self-Consistent Equations Including Exchange and Correlation Effects. *Phys. Rev.* **1965**, *140*, A1133–A1138.

- (23) Wang, V.; Xu, N.; Liu, J.-C.; Tang, G.; Geng, W.-T. VASPKIT: A user-friendly interface facilitating high-throughput computing and analysis using VASP code. *Computer Physics Communications* **2021**, *267*, 108033.
- (24) Perdew, J. P.; Burke, K.; Ernzerhof, M. Generalized Gradient Approximation Made Simple. *Phys. Rev. Lett.* **1996**, *77*, 3865–3868.
- (25) Grimme, S.; Antony, J.; Ehrlich, S.; Krieg, H. A consistent and accurate ab initio parametrization of density functional dispersion correction (DFT-D) for the 94 elements H-Pu. *The Journal of Chemical Physics* **2010**, *132*, 154104.
- (26) Dudarev, S. L.; Botton, G. A.; Savrasov, S. Y.; Humphreys, C. J.; Sutton, A. P. Electron-energy-loss spectra and the structural stability of nickel oxide: An LSDA+U study. *Phys. Rev. B* **1998**, *57*, 1505–1509.
- (27) Yang, K.; Wang, G.; Liu, L.; Lu, D.; Wu, H. Triaxial magnetic anisotropy in the two-dimensional ferromagnetic semiconductor CrSBr. *Phys. Rev. B* **2021**, *104*, 144416.
- (28) Carrete, J.; Vermeersch, B.; Katre, A.; van Roekeghem, A.; Wang, T.; Madsen, G. K.; Mingo, N. almaBTE : A solver of the spacetime dependent Boltzmann transport equation for phonons in structured materials. *Computer Physics Communications* **2017**, *220*, 351–362.
- (29) Togo, A. First-principles Phonon Calculations with Phonopy and Phono3py. *J. Phys. Soc. Jpn.* **2023**, *92*, 012001.
- (30) Eriksson, F.; Fransson, E.; Erhart, P. The Hiphive Package for the Extraction of High-Order Force Constants by Machine Learning. *Adv. Theory Simul.* **2019**, *2*, 1800184.
- (31) Carrete, J.; Li, W.; Lindsay, L.; Broido, D. A.; Gallego, L. J.; Mingo, N. Physically founded phonon dispersions of few-layer materials and the case of borophene. *Mater. Res. Lett.* **2016**, *4*, 204–211.

- (32) Sánchez-Portal, D.; Hernández, E. Vibrational properties of single-wall nanotubes and monolayers of hexagonal BN. *Phys. Rev. B* **2002**, *66*, 235415.
- (33) Sohler, T.; Gibertini, M.; Calandra, M.; Mauri, F.; Marzari, N. Breakdown of Optical Phonons' Splitting in Two-Dimensional Materials. *Nano Lett.* **2017**, *17*, 3758–3763.
- (34) De Luca, M.; Cartoixà, X.; Indolese, D. I.; Martín-Sánchez, J.; Watanabe, K.; Taniguchi, T.; Schönenberger, C.; Trotta, R.; Ruruli, R.; Zardo, I. Experimental demonstration of the suppression of optical phonon splitting in 2D materials by Raman spectroscopy. *2D Mater.* **2020**, *7*, 035017.
- (35) Guo, Y.; Zhang, Y.; Yuan, S.; Wang, B.; Wang, J. Chromium sulfide halide monolayers: intrinsic ferromagnetic semiconductors with large spin polarization and high carrier mobility. *Nanoscale* **2018**, *10*, 18036–18042.
- (36) Rudenko, A. N.; Rösner, M.; Katsnelson, M. I. Dielectric tunability of magnetic properties in orthorhombic ferromagnetic monolayer CrSBr. *npj Comput. Mater.* **2023**, *9*, 83.
- (37) Wang, H.; Qi, J.; Qian, X. Electrically tunable high Curie temperature two-dimensional ferromagnetism in van der Waals layered crystals. *Appl. Phys. Lett.* **2020**, *117*, 083102.
- (38) Zhou, X.; Zhou, B. Enhanced Curie temperature of ferromagnetic CrSBr by interfacial coupling with elemental two-dimensional ferroelectrics: triggering a new p-d superexchange coupling path. *Phys. Chem. Chem. Phys.* **2025**, *27*, 20500–20508.
- (39) Fugallo, G.; Colombo, L. Calculating lattice thermal conductivity: a synopsis. *Phys. Scr.* **2018**, *93*, 043002.
- (40) Cepellotti, A.; Fugallo, G.; Paulatto, L.; Lazzeri, M.; Mauri, F.; Marzari, N. Phonon hydrodynamics in two-dimensional materials. *Nature Communications* **2015**, *6*, 6400.

- (41) Fugallo, G.; Cepellotti, A.; Paulatto, L.; Lazzeri, M.; Marzari, N.; Mauri, F. Thermal Conductivity of Graphene and Graphite: Collective Excitations and Mean Free Paths. *Nano Letters* **2014**, *14*, 6109–6114, PMID: 25343716.
- (42) Torres, P.; Alvarez, F. X.; Cartoixà, X.; Rurali, R. Thermal conductivity and phonon hydrodynamics in transition metal dichalcogenides from first-principles. *2D Materials* **2019**, *6*, 035002.
- (43) Ding, Z.; Zhou, J.; Song, B.; Li, M.; Liu, T.-H.; Chen, G. Umklapp scattering is not necessarily resistive. *Phys. Rev. B* **2018**, *98*, 180302.
- (44) Torres, P.; Torelló, A.; Bafaluy, J.; Camacho, J.; Cartoixà, X.; Alvarez, F. X. First principles kinetic-collective thermal conductivity of semiconductors. *Phys. Rev. B* **2017**, *95*, 165407.
- (45) Cepellotti, A.; Marzari, N. Thermal Transport in Crystals as a Kinetic Theory of Relaxons. *Phys. Rev. X* **2016**, *6*, 041013.